The orbits and masses of satellites of Pluto

Marina Brozović [a,*], Mark R. Showalter [b], Robert A. Jacobson [a], Marc W. Buie [c]

[a] Jet Propulsion Laboratory, California Institute of Technology, Pasadena, CA 91109-8099, USA
[b] SETI, Mountain View, CA 94043, USA
[c] SWRI, Boulder, CO 80302, USA

ABSTRACT

We present the numerically integrated orbits of Pluto's satellites. The orbits have been fit to a data set that includes Earth-based and Hubble Space Telescope (HST) astrometry of Charon, Nix, Hydra, Kerberos, and Styx, as well as the lightcurves from the Pluto–Charon mutual events. We also report new, 2010–2012 HST astrometry of all satellites including recently discovered Styx plus a pre-discovery detection of Kerberos in 2006. Pluto-relative data sets have been corrected for the center-of-light vs. center-of-mass offsets with the Pluto albedo model. The results are summarized in terms of the postfit residuals, state vectors, and mean orbital elements. Orbits of Charon, Styx, Nix, and Kerberos are nearly circular, while Hydra's shows a small eccentricity. All satellites are in near-resonance conditions, but we did not uncover any resonant arguments. Our model yields 975.5 ± 1.5 km^3 s^{-2}, 869.6 ± 1.8 km^3 s^{-2}, and 105.9 ± 1.0 km^3 s^{-2} for the system's, Pluto's, and Charon's GM values. The uncertainties reflect both systematic and random measurement errors. The GM values imply a bulk density of 1.89 ± 0.06 g cm^{-3} for Pluto and 1.72 ± 0.02 g cm^{-3} for Charon. We also obtain GM$_{Nix}$ = 0.0030 ± 0.0027 km^3 s^{-2} GM$_{Hydra}$ = 0.0032 ± 0.0028 km^3 s^{-2}, GM$_{Kerberos}$ = 0.0011 ± 0.0006 km^3 s^{-2}, and an upper bound on Styx's GM of 0.0010 km^3 s^{-2}. The 1σ errors are based on the formal covariance from the fit and they reflect only measurement errors. In-orbit (or along the track), radial, and out-of-plane orbital uncertainties at the time of New Horizons encounter are on the order of few tens of km or less for Charon, Nix, and Hydra. Kerberos and Styx have their largest uncertainty component of $\sim$140 km and $\sim$500 km respectively in the in-orbit direction.

© 2014 Elsevier Inc. All rights reserved.

1. Introduction

Dwarf-planet Pluto and its five currently known satellites (Charon, Nix, Hydra, Kerberos, and Styx) are the highly anticipated targets of NASA's New Horizons mission in 2015. Not only was Pluto once considered the ninth planet of the Solar System, but it is also the first discovered Kuiper belt object (KBO). New Horizons will be able to obtain unprecedented science data on the Pluto system that are likely to surprise and excite astronomers. Good-quality orbital solutions for Pluto and its satellites are the important prerequisites for the mission's success. Here, we provide the latest orbits and mass estimates for Pluto's satellites based on the most complete data set to date.

Charon was discovered in 1978 by James Christy (Christy and Harrington, 1978), and since then there have been multiple studies (Tholen et al., 1987, 2008; Foust et al., 1997; Tholen and Buie, 1997; Olkin et al., 2003; Buie et al., 2006; Lee and Peale, 2006; Sicardy et al., 2011; Beauvalet et al., 2013) to establish its orbit and mass ratio with respect to Pluto. Charon's orbit around Pluto is nearly circular, and the pair is tidally locked. Buie et al. (2012) reported that the upper limit to Charon's eccentricity is 7.5×10^{-5}. Early estimates of the Pluto–Charon mass ratio (r = GM$_{Charon}$/GM$_{Pluto}$) varied substantially, from r = 0.0837 ± 0.0147 (Null et al., 1993) to r = 0.1566 ± 0.0035 (Young et al., 1994). Two later estimates by Buie et al. (2006) and Tholen et al. (2008) have very consistent values: r = 0.1165 ± 0.0055 and r = 0.1166 ± 0.0069, respectively. The most recent analysis (Beauvalet et al., 2013) lists two ratios for the two sets of Pluto–Charon masses. Their more complete dataset gives r = 0.1126 ± 0.0001, while the one that excludes the Buie et al. (2012) data gives r = 0.1176 ± 0.0022. Two findings are apparent: Buie et al. (2012) data have significantly lowered the mass estimate for Charon (from GM$_{Charon}$ = 102.83 ± 1.87 km^3 s^{-2} to GM$_{Charon}$ = 98.33 ± 0.11 km^3 s^{-2}) and the added data have also significantly reduced the uncertainty on the mass of Charon. It is important to note that these uncertainties only reflect measurement errors as opposed to any systematic errors.

Weaver et al. (2006) were the first to attempt to determine orbital parameters for Nix and Hydra (originally S/2005 (134340) 2 and S/2005 (134340) 1) based on a few discovery data points. Although the data set turned out to be too sparse to allow definite determination of the orbits, they concluded that the two satellites appeared to be moving in circular orbits in the same orbital plane as Charon. Orbital periods were estimated to be ~25 days for Nix and ~38 days for Hydra. Buie et al. (2006) followed with a two-body orbit solution in the Pluto–Charon barycentric frame. They confirmed that the orbits of all three satellites are nearly coplanar, and they found that the orbit of Hydra has an eccentricity of $e_{Hydra} = 0.0052 \pm 0.0011$.

Lee and Peale (2006) presented a theoretical study of the orbits of Nix and Hydra. They first discussed an analytic theory, which they followed with integrated orbits for various considerations of the satellites' masses. The range of masses was calculated based on the assumption that the geometric albedo is either similar to that of Charon (high-albedo–low-mass) or to that of a comet (low-albedo–high-mass). For the case where the masses of Nix and Hydra were low, Lee and Peale (2006) predicted that Hydra has a significant epicyclic eccentricity and that the prograde precession of its longitude of periapsis has a period of ~5300 days. At the high end of the albedo-derived masses (a geometric albedo of few percent), Lee and Peale (2006) found that Nix and Hydra could be in the 3:2 mean-motion resonance (the resonant parameter $\theta_{Hydra} = 2\phi_{Nix} - 3\phi_{Hydra} + \varpi_{Hydra}$ librating about 180 deg) with the Hydra's longitude of periapsis (ϖ_{Hydra}) in retrograde precession with a 500-day period.

Tholen et al. (2008) were the first to attempt a four-body orbital fit to the data and they obtained order-of-magnitude GM estimates for Nix and Hydra: $GM_{Nix} = 0.039 \pm 0.034$ km^3 s^{-2} and $GM_{Hydra} = 0.021 \pm 0.042$ km^3 s^{-2}. Their analysis also ruled out the high end of Nix and Hydra masses that Lee and Peale (2006) found as a necessary condition in order to have 3:2 mean-motion resonance. Beauvalet et al. (2013) reported the most recent integrated orbital fit to the astrometry of the satellites in the Pluto system. Their results placed tighter constraints on the masses of Nix and Hydra ($GM_{Nix} = 0.014 \pm 0.011$ km^3 s^{-2} and $GM_{Hydra} = 0.069 \pm 0.014$ km^3 s^{-2}), although the dataset that they used was still relatively sparse and potentially sensitive to the systematic effects in the data.

The latest additions to the Pluto family are satellites Kerberos (S/2011 (134340) 1) (Showalter et al., 2011) and Styx (S/2012 (134340) 1) (Showalter et al., 2012). Not much is known about these satellites, except that they orbit Pluto in nearly circular orbits with $a_{Styx} \sim 42{,}000$ km (Showalter et al., 2012) and $a_{Kerberos} \sim 57{,}900$ km (Buie et al., 2013). Their respective periods are $P_{Styx} \sim 20.1$ days and $P_{Kerberos} \sim 32.2$ days. Together with Nix and Hydra, Styx and Kerberos complete the continuous sequence of near-resonant orbits (1:3:4:5:6) with respect to Pluto–Charon orbital period.

The question of dynamical stability and the number of satellites in the Pluto system was discussed long before the Nix and Hydra discovery (Stern et al., 1994). Stern et al. (1994) showed that there is a region of space around Charon (so-called instability strip) that is unlikely to contain any other satellites because their orbits would be unstable. However, the regions interior and exterior to the Charon's instability strip were not excluded for the existence of small satellites (masses up to 10^{-4} of the Pluto–Charon GM). Furthermore, Stern et al. (1994) found that at two Pluto–Charon separation distances, it is possible to consider the existence of even more massive satellites (masses up to 10^{-2} of the Pluto–Charon GM). The discovery of Nix and Hydra in the same orbital plane as Charon and in the proximity of 4:1 and 6:1 mean motion resonances with Pluto–Charon orbital period led to some interesting studies on the stability of their orbits. Süli and Zsigmond (2009) used the spatial elliptic restricted three-body problem to study the dynamical structure of the phase space around Nix and Hydra

and they found that Nix could be in 4:1 resonance for a certain selection of arguments of periapsis and longitudes of node, but that there are no combinations that could put Hydra in 6:1 resonance. Pires dos Santos et al. (2011) have analyzed the dynamical stability of the region beyond Charon in the light of Nix and Hydra perturbations. They concluded that the potential satellites would have to reside either as coorbitals of Nix and Hydra or between their orbits. The discovery of Styx and Kerberos in 3:1 and 5:1 near-resonance further raised the complexity of the Pluto system's dynamical architecture, but it also provided some tighter constraints for the masses in the system. For example, Youdin et al. (2012) used the orbit of the newly discovered Kerberos to explore the system's long-term stability in 4 + N body integrations (the four massive bodies are Pluto, Charon, Nix, and Hydra). This analysis constrained the masses of Nix and Hydra to an upper limit of 5×10^{16} kg (0.0033 km^3 s^{-2}) and 9×10^{16} kg (0.0060 km^3 s^{-2}), respectively. Furthermore, Youdin et al. (2012) have also predicted that the orbit of Kerberos lies just exterior to the 5:1 resonance. Most recently, Kenyon and Bromley (2014) did a numerical study of how the small satellites coagulated and migrated in a disk of debris particles around the newly formed Pluto–Charon binary and one of the conclusions was that there could be more small satellites (with radii between 1 and 3 km) beyond the orbit of Hydra.

2. Observations and data reduction

2.1. Old astrometry

We used the most complete set of Charon, Nix, Hydra, Kerberos, and Styx astrometry to date. The data include both Earth-based and HST observations as well as the lightcurves from Pluto–Charon mutual events. Table 1 shows that the earliest Charon data (Harrington and Christy, 1980) originated from photographic plates taken between 1965 and 1979. Charon's position (in position angle $\Delta\theta$ and separation $\Delta\rho$) is given relative to Pluto. The data before June 22, 1978 predate Charon's discovery (Christy and Harrington, 1978). Speckle interferometry provided early-to-mid-1980s measurements of the relative positions of Pluto and Charon (Bonneau and Foy, 1980; Hege et al., 1982; Hege and Drummond, 1984; Hetterich and Weigelt, 1983; Baier et al., 1982; Baier and Weigelt, 1987; Beletic et al., 1989). Beletic et al. (1989) measured Charon's position as separation in right-ascension ($\Delta\alpha$) projected onto a tangential plane (thus multiplied by cosine of declination) and separation in declination ($\Delta\delta$). All other measurements were position angle and separation from Pluto. Both photographic plates and speckle interferometry data have accuracies of ~100 milliarcseconds (mas).

The first HST astrometry was obtained in 1991 by Null et al. (1993); they measured absolute positions of Charon and Pluto in terms of samples and lines with the Wide-Field/Planetary Camera (WFPC). Follow up HST astrometry was obtained by Null and Owen in 1992–1993 (Null and Owen, 1996). At the same time, Tholen and Buie (1997) used HST to measure relative positions of Pluto and Charon in terms of $\Delta\theta$ and $\Delta\rho$. These data were later corrected with Pluto's albedo model (Buie et al., 2012) and expressed in terms of $\Delta\alpha\cos(\delta)$ and $\Delta\delta$.

Earth-based measurements of the Pluto system resumed in 1992 when Young et al. (1994) obtained Charon's location relative to Pluto ($\Delta\alpha$, $\Delta\delta$) with Mauna Kea's Observatory (MKO) 2.2 m telescope. The accuracy of these measurements is on the order 10–30 mas. Olkin et al. (2003) used HST in 1998 to determine absolute positions (α, δ) of Pluto and Charon. Buie et al. (2006) obtained an extensive HST dataset of relative positions of Pluto and Charon ($\Delta\theta$ and $\Delta\rho$) during 2002–2003. They reported 384 data points measured over 12 separate HST "visits" that were scheduled to map out the surface features as Pluto rotates. The stacked HST images also contain 12

Table 1
Observations of Charon.

Time span	Type	Points	rms (arcsec)	Type	Points	rms (arcsec)	References
April 1965–April 1979	$\rho\Delta\theta$	23	0.105	$\Delta\rho$	12	0.146	Harrington and Christy (1980)
June 1980–February 1984	$\rho\Delta\theta$	2	0.019	$\Delta\rho$	2	0.083	Hege et al. (1982) and Hege and Drummond (1984)
June 1980	$\rho\Delta\theta$	5	0.015	$\Delta\rho$	5	0.029	Bonneau and Foy (1980)
April 1981	$\rho\Delta\theta$	2	0.011	$\Delta\rho$	2	0.022	Hetterich and Weigelt (1983)
April 1981–July 1983	$\rho\Delta\theta$	8	0.041	$\Delta\rho$	8	0.082	Baier et al. (1982) and Baier and Weigelt (1987)
May 1984–1985	$\Delta\alpha\cos(\delta)$	56	0.087	$\Delta\delta$	56	0.073	Beletic et al. (1989)
August 1991–1993	Sample	28	0.007	Line	28	0.007	Null et al. (1993) and Null and Owen (1996)
May 1992–August 1993	$\Delta\alpha\cos(\delta)$	60	0.003	$\Delta\delta$	60	0.003	Tholen and Buie (1997) and Buie et al. (2012)
February 1992–March 1992	$\Delta\alpha\cos(\delta)$	80	0.029	$\Delta\delta$	80	0.011	Young et al. (1994)
March 1998	α	5	0.014	δ	5	0.015	Olkin et al. (2003)
June 2002–2003	$\Delta\alpha\cos(\delta)$	384	0.002	$\Delta\delta$	384	0.002	Buie et al. (2006, 2012)
June 2005	$\Delta\alpha\cos(\delta)$	45	0.001	$\Delta\delta$	45	<0.001	Sicardy et al. (private communication)
May 2005	$\rho\Delta\theta$	2	0.020	$\Delta\rho$	2	0.007	Weaver et al. (2006)
April 2006	$\Delta\alpha\cos(\delta)$	1	0.001	$\Delta\delta$	1	0.002	Sicardy et al. (2006a)
February 2006	$\Delta\alpha\cos(\delta)$	10	0.004	$\Delta\delta$	10	0.003	Showalter (this paper)
March 2007–June 2007	$\Delta\alpha\cos(\delta)$	215	0.002	$\Delta\delta$	215	0.003	Buie et al. (2012)
June 2008–2011	$\Delta\alpha\cos(\delta)$	2	0.001	$\Delta\delta$	2	<0.001	Sicardy et al. (2011, private communication)
April 2010–September 2010	$\Delta\alpha\cos(\delta)$	95	0.003	$\Delta\delta$	95	0.002	Showalter (this paper)
April 2010–September 2010	$\Delta\alpha\cos(\delta)$	240	0.003	$\Delta\delta$	240	0.002	Buie et al. (2012)
June 2011–September 2011	$\Delta\alpha\cos(\delta)$	104	0.003	$\Delta\delta$	104	0.002	Showalter (this paper)
June 2012–July 2012	$\Delta\alpha\cos(\delta)$	548	0.002	$\Delta\delta$	548	0.002	Showalter (this paper)
July 2012	$\rho\Delta\theta$	1	0.002	$\Delta\rho$	1	0.001	Howell et al. (2012)

Masterlog of Charon's astrometry. The table lists the time span for the observations as well as the type of measurement, the number of the astrometry points, and the rms of the residuals (in arcseconds) obtained from our orbital fit. The astrometry reported as ($\Delta\theta$, $\Delta\rho$) are relative measurements of Charon with respect to Pluto in terms of the position angle and separation, the rms of the residuals is listed as ($\rho\Delta\theta$, $\Delta\rho$). The astrometry reported as ($\Delta\alpha\cos(\delta)$, $\Delta\delta$) are relative measurements of Charon with respect to Pluto (or a reference position for Pluto for the new astrometry (Section 2.2)) in terms of the right ascension projected onto a tangential plane and declination. The oldest HST data (Null et al., 1993; Null and Owen, 1996) are in (Sample, Line) format and these are the absolute measurements of Charon's position. In addition, Olkin et al. (2003) HST data (α, δ) are also absolute measurements of Charon's position.

detections of Nix and Hydra that predate the discovery of these satellites. Buie et al. (2012) continued observing the Pluto system with HST in 2007 and 2010, and they have reported several hundred relative astrometry points with 3–4 mas accuracy.

The last substantial dataset (45 points) of ground observations of the Pluto–Charon relative positions was reported by Sicardy et al. (Sicardy, private communication). The astrometry was obtained in June of 2005 with adaptive optics system NACO/VLT at Paranal. There exist a few more Charon data points: there are 2 HST measurements by Weaver et al. (2006) from their 2005 discovery of Nix and Hydra and one more point by Sicardy (2006a) from the time when Hydra was re-observed with NACO/VLT at Paranal. Two very precise astrometric points (∼0.3 mas precision) were obtained from the dual stellar occultations of Pluto and Charon on June 22, 2008 (Sicardy et al., 2011) and on June 4, 2011 (Sicardy, private communication). This was an exceptional opportunity to constrain the orbit of Charon by directly measuring the distance between Pluto and Charon in the plane of sky. The last ground based astrometry points came from the speckle interferometric Pluto–Charon relative positions from Howell et al. (2012).

Our data set also contains 64 lightcurves from the 1985–1990 period when the viewing geometry from Earth was favorable to observe the mutual events between Pluto and Charon. We used the EAR-A-3-RDR-PCME-V3.0 dataset (Tholen, 2008, http://pds.nasa.gov/ds-view/pds/viewDataset.jsp?dsid=EAR-A-3-RDR-PCME-V3.0) that contains 15 lightcurves from Palomar (Buratti et al., 1995), 39 lightcurves from Mauna Kea Observatory (Tholen, 2008), and 10 lightcurves from McDonald Observatory (Young, 1992; Young and Binzel, 1993).

Tables 2–5 list all available astrometry for Nix, Hydra, Kerberos, and Styx. Almost all measurements were obtained with the HST, with the exception of the Sicardy et al. (2006a) and Fuentes and Holman (2006) data points that were obtained with NACO/VLT and Magelan I Baade telescopes. The data set includes the discovery points from 2005 by Weaver et al. (2006) as well as the pre-discovery points by Buie et al. (2006). All measurements are relative positions of Nix, Hydra, Kerberos, and Styx with respect to Pluto or Charon. We note that

all astrometry in Buie et al. (2013) was reported with respect to the barycenter determined by Tholen et al. (2008) orbital fit. For the purpose of this analysis, we re-measured all the data with respect to Charon. This makes the data set more general, as well as it simplifies the input into our orbital fitting software.

2.2. New astrometry

For this paper, we have obtained new HST astrometry of Pluto and all five known satellites spanning 2010–2012, all obtained with the UVIS channel of the Wide Field Camera 3 (WFC3). We have also obtained measurements of a pre-discovery detection of Kerberos from 2006 using HST's High Resolution Channel (HRC) of the Advanced Camera for Surveys (ACS). Table 1 in Supplementary material summarizes all of the images used in this analysis, and Tables 2–5 in Supplementary material contain all the new measurements (a sample of the new measurements is shown in Table 6). Note that this data set overlaps with that of Buie et al. (2013); Pluto, Charon, Nix and Hydra have been re-measured in the images prior to 2011. The new measurements of Kerberos expand upon the earlier work by Buie et al. (2013).

Pluto is currently located in front of a dense star field in Sagittarius. The HST images are lengthy exposures tracking Pluto, causing background stars to smear out into long trails. These must be suppressed in order to detect the satellites. We take advantage of the fact that the satellites are essentially stationary relative to Pluto within the ∼45-min observing window of a single HST orbit. We process the images by aligning Pluto in all the images from the same orbit, forming a "stack" of images that would be essentially identical if not for the background stars streaming through the field of view. We then sort the pixels at each overlapping location in the stack, from dimmest to brightest. This causes the stars to "rise to the top", where they can be easily identified as anomalously bright relative to the median value at each location. The anomalous pixels are masked out, and the remainders are averaged together. In this way, we obtain clean, star-free images in which the smallest moons can be detected.

Table 2
Observations of Nix.

Time span	Type	Points	rms (arcsec)	Type	Points	rms (arcsec)	References
June 2002–2003	$\Delta\alpha\cos(\delta)$	11	0.017	$\Delta\delta$	11	0.011	Buie et al. (2006, 2013)
May 2005	$\rho\Delta\theta$	2	0.015	$\Delta\rho$	2	0.022	Weaver et al. (2006)
February 2006	$\rho\Delta\theta$	1	0.030	$\Delta\rho$	1	0.011	Mutchler et al. (2006)
March 2006	$\rho\Delta\theta$	1	0.012	$\Delta\rho$	1	0.011	Stern et al. (2006)
June 2006	$\Delta\alpha\cos(\delta)$	2	0.126	$\Delta\delta$	2	0.122	Fuentes and Holman (2006)
March 2007–June 2007	$\Delta\alpha\cos(\delta)$	149	0.005	$\Delta\delta$	149	0.005	Buie et al. (2013)
April 2010–September 2010	$\Delta\alpha\cos(\delta)$	45	0.004	$\Delta\delta$	45	0.005	Buie et al. (2013)
April 2010–September 2010	$\Delta\alpha\cos(\delta)$	88	0.004	$\Delta\delta$	88	0.004	Showalter (this paper)
June 2011–September 2011	$\Delta\alpha\cos(\delta)$	145	0.005	$\Delta\delta$	145	0.006	Showalter (this paper)
June 2012–July 2012	$\Delta\alpha\cos(\delta)$	630	0.003	$\Delta\delta$	630	0.004	Showalter (this paper)

Masterlog of Nix's astrometric observations and their orbital fit residual rms. The table follows the same convention as Table 1. All data are relative to Pluto (or a reference position for Pluto for the new astrometry (Section 2.2)), except Buie et al. (2013) data which are relative to Charon.

Table 3
Observations of Hydra.

Time span	Type	Points	rms (arcsec)	Type	Points	rms (arcsec)	References
June 2002–2003	$\Delta\alpha\cos(\delta)$	11	0.010	$\Delta\delta$	11	0.010	Buie et al. (2006, 2013)
May 2005	$\rho\Delta\theta$	2	0.011	$\Delta\rho$	2	0.026	Weaver et al. (2006)
February 2006	$\rho\Delta\theta$	1	0.001	$\Delta\rho$	1	0.003	Mutchler et al. (2006)
March 2006	$\rho\Delta\theta$	1	0.004	$\Delta\rho$	1	0.004	Stern et al. (2006)
April 2006	$\Delta\alpha\cos(\delta)$	1	0.021	$\Delta\delta$	1	0.006	Sicardy et al. (2006a)
June 2006	$\Delta\alpha\cos(\delta)$	2	0.124	$\Delta\delta$	2	0.086	Fuentes and Holman (2006)
March 2007–June 2007	$\Delta\alpha\cos(\delta)$	149	0.003	$\Delta\delta$	149	0.005	Buie et al. (2013)
April 2010–September 2010	$\Delta\alpha\cos(\delta)$	44	0.004	$\Delta\delta$	44	0.004	Buie et al. (2013)
April 2010–September 2010	$\Delta\alpha\cos(\delta)$	87	0.003	$\Delta\delta$	87	0.003	Showalter (this paper)
June 2011–September 2011	$\Delta\alpha\cos(\delta)$	151	0.003	$\Delta\delta$	151	0.003	Showalter (this paper)
June 2012–July 2012	$\Delta\alpha\cos(\delta)$	622	0.003	$\Delta\delta$	622	0.003	Showalter (this paper)

Masterlog of Hydra's astrometric observations and their orbital fit residual rms. The table follows the same convention as Table 1. All data are relative to Pluto (or a reference position for Pluto for the new astrometry (Section 2.2)), except Buie et al. (2013) data which are relative to Charon.

Table 4
Observations of Kerberos.

Time span	Type	Points	rms (arcsec)	Type	Points	rms (arcsec)	References
May 2005	$\rho\Delta\theta$	2	0.029	$\Delta\rho$	2	0.093	Steffl et al. (2011, private communication)
February 2006	$\Delta\alpha\cos(\delta)$	4	0.032	$\Delta\delta$	3	0.004	Showalter (this paper)
April 2010–September 2010	$\Delta\alpha\cos(\delta)$	37	0.017	$\Delta\delta$	37	0.013	Buie et al. (2013)
April 2010–September 2010	$\Delta\alpha\cos(\delta)$	35	0.011	$\Delta\delta$	35	0.011	Showalter (this paper)
June 2011–September 2011	$\Delta\alpha\cos(\delta)$	30	0.009	$\Delta\delta$	30	0.009	Showalter (this paper)
June 2012–July 2012	$\Delta\alpha\cos(\delta)$	129	0.013	$\Delta\delta$	129	0.015	Showalter (this paper)

Masterlog of Kerberos's astrometric observations and their orbital fit residual rms. The table follows the same convention as Table 1. All data are relative to Pluto (or a reference position for Pluto for the new astrometry (Section 2.2)), except Buie et al. (2013) data which are relative to Charon.

Table 5
Observations of Styx.

Time span	Type	Points	rms (arcsec)	Type	Points	rms (arcsec)	References
April 2010–September 2010	$\Delta\alpha\cos(\delta)$	7	0.017	$\Delta\delta$	7	0.013	Showalter (this paper)
June 2011–September 2011	$\Delta\alpha\cos(\delta)$	15	0.028	$\Delta\delta$	15	0.020	Showalter (this paper)
June 2012–July 2012	$\Delta\alpha\cos(\delta)$	37	0.030	$\Delta\delta$	37	0.031	Showalter (this paper)

Masterlog of Styx's astrometric observations and their orbital fit residual rms. The table follows the same convention as Table 1. All data are relative to a reference position for Pluto (Section 2.2).

Our astrometry procedure is similar to that of Buie et al. (2013). All measurements are necessarily relative, not absolute, because the background stars have been eliminated; this is typical for Earth-based astrometry of regular satellite systems. For each image, we used the "Tiny Tim" software (Krist et al., 2011), which is supported by the Space Telescope Science Institute, to generate model point spread functions (PSFs) for an unresolved object in the field of view of each image. The precise shape of the PSF varies from place to place within each HST field of view, but because the Pluto system is so compact on the sky, we were able to use a single PSF for each image, based on the approximate location of Pluto on the chip. The model PSF from Tiny Tim was sampled on a grid four times finer than the UVIS or HRC pixel scale, so that we could shift the PSF at the sub-pixel level and then resample it to the CCD's resolution, all the while avoiding any significant loss of precision.

Individual measurements were obtained by fitting the model PSF to a square of pixels surrounding the planet or a satellite. Using nonlinear least squares fitting, we obtained the central (x, y) position of the body plus an overall scaling factor on the PSF to account for the body's brightness. Where necessary to accommodate the

Table 6
2010 HST observations of Pluto's satellites.

Image ID	Mid-time (UTC)	Body	Δαcos(δ) (arcsec)	σ (arcsec)	Δδ (arcsec)	σ (arcsec)	x (pixel)	σ (pixel)	y (pixel)	σ (pixel)
IB4W01I5Q	2010-04-24T07:28:22.5	Charon	0.52175	0.00017	0.32192	0.00017	270.144	0.004	262.077	0.004
IB4W01I6Q	2010-04-24T07:29:52.5	Charon	0.52465	0.00024	0.32495	0.00024	272.736	0.006	264.597	0.006
IB4W01I7Q	2010-04-24T07:31:32.5	Charon	0.52333	0.00022	0.32318	0.00022	271.714	0.005	262.054	0.005
IB4W01I8Q	2010-04-24T07:33:22.5	Charon	0.52547	0.00025	0.32002	0.00025	274.174	0.006	264.669	0.006
IB4W01IJQ	2010-04-24T07:58:37.5	Charon	0.53185	0.00023	0.30874	0.00023	271.823	0.006	263.725	0.006
IB4W01IKQ	2010-04-24T08:00:27.5	Charon	0.53291	0.00024	0.30875	0.00024	274.327	0.006	266.265	0.006
IB4W01INQ	2010-04-24T08:11:35.5	Charon	0.54039	0.00028	0.30121	0.00028	270.297	0.007	264.044	0.007
IB4W01IOQ	2010-04-24T08:13:05.5	Charon	0.53985	0.00027	0.30032	0.00027	272.758	0.007	266.570	0.007
IB4W02FMQ	2010-05-21T16:14:02.5	Charon	0.32269	0.00024	−0.80099	0.00024	249.875	0.006	277.618	0.006
IB4W02FNQ	2010-05-21T16:15:32.5	Charon	0.32246	0.00022	−0.80207	0.00022	252.337	0.006	280.152	0.005
IB4W01I7Q	2010-04-24T07:31:32.5	Nix	0.06944	0.00314	−1.89881	0.00314	221.776	0.098	292.926	0.055
IB4W01I8Q	2010-04-24T07:33:22.5	Nix	0.06939	0.00280	−1.90368	0.00280	224.169	0.067	295.532	0.074
IB4W01I9Q	2010-04-24T07:36:39.5	Nix	0.07018	0.00111	−1.89736	0.00111	224.823	0.027	292.635	0.029
IB4W01IAQ	2010-04-24T07:41:23.5	Nix	0.06773	0.00113	−1.89799	0.00113	227.258	0.028	295.122	0.030
IB4W01IJQ	2010-04-24T07:58:37.5	Nix	0.06108	0.00258	−1.89467	0.00258	221.968	0.068	293.960	0.061
IB4W01IKQ	2010-04-24T08:00:27.5	Nix	0.06161	0.00308	−1.89302	0.00308	224.496	0.078	296.462	0.077
IB4W01ILQ	2010-04-24T08:03:44.5	Nix	0.06302	0.00143	−1.89594	0.00143	224.983	0.036	293.740	0.036
IB4W01IMQ	2010-04-24T08:08:28.5	Nix	0.05978	0.00203	−1.89688	0.00203	227.400	0.052	296.218	0.051
IB4W02FOQ	2010-05-21T16:17:12.5	Nix	−0.96353	0.00210	−1.32706	0.00210	221.881	0.058	260.788	0.047
IB4W02FPQ	2010-05-21T16:19:02.5	Nix	−0.98129	0.00210	−1.32630	0.00210	224.124	0.054	262.947	0.052
IB4W01I7Q	2010-04-24T07:31:32.5	Hydra	−0.59220	0.00165	2.70479	0.00165	299.330	0.044	199.607	0.038
IB4W01I8Q	2010-04-24T07:33:22.5	Hydra	−0.58989	0.00164	2.70321	0.00164	301.823	0.044	202.197	0.039
IB4W01I9Q	2010-04-24T07:36:39.5	Hydra	−0.59062	0.00059	2.70148	0.00059	302.297	0.015	199.417	0.015
IB4W01IAQ	2010-04-24T07:41:23.5	Hydra	−0.58733	0.00055	2.70263	0.00055	304.859	0.013	201.977	0.015
IB4W01IJQ	2010-04-24T07:58:37.5	Hydra	−0.58522	0.00413	2.70279	0.00413	299.653	0.107	201.031	0.101
IB4W01IKQ	2010-04-24T08:00:27.5	Hydra	−0.58671	0.00287	2.70782	0.00287	302.211	0.071	203.434	0.074
IB4W01ILQ	2010-04-24T08:03:44.5	Hydra	−0.57975	0.00050	2.70249	0.00050	302.740	0.013	200.858	0.012
IB4W01IMQ	2010-04-24T08:08:28.5	Hydra	−0.57951	0.00067	2.70099	0.00067	305.202	0.016	203.409	0.018
IB4W02FOQ	2010-05-21T16:17:12.5	Hydra	−1.99561	0.00149	−0.63208	0.00149	220.968	0.030	229.271	0.044
IB4W02FPQ	2010-05-21T16:19:02.5	Hydra	−1.99589	0.00138	−0.62635	0.00138	223.567	0.036	231.693	0.033
IB4W01I9Q	2010-04-24T07:36:39.5	Kerberos	−0.47994	0.00712	−1.99204	0.00712	214.116	0.177	284.214	0.182
IB4W01IAQ	2010-04-24T07:41:23.5	Kerberos	−0.49128	0.00741	−1.99961	0.00741	216.275	0.195	286.661	0.178
IB4W01IBQ	2010-04-24T08:03:44.5	Kerberos	−0.49992	0.01871	−1.98377	0.01871	214.199	0.512	284.963	0.427
IB4W02FQQ	2010-05-21T16:22:19.5	Kerberos	1.31062	0.00619	−2.34035	0.00619	237.461	0.162	321.606	0.150
IB4W03FBQ	2010-05-24T22:39:19.5	Kerberos	0.00709	0.00647	−2.24375	0.00647	217.973	0.158	294.120	0.169
IB4W03FCQ	2010-05-24T22:44:03.5	Kerberos	0.02841	0.00622	−2.25018	0.00622	220.632	0.156	297.168	0.157
IB4W03FNQ	2010-05-24T23:06:24.5	Kerberos	0.03016	0.00517	−2.24166	0.00517	218.594	0.137	295.808	0.123
IB4W03FOQ	2010-05-24T23:11:08.5	Kerberos	−0.02097	0.01019	−2.25311	0.01019	220.115	0.271	297.491	0.242
IB4W04J5Q	2010-06-01T22:40:14.5	Kerberos	−1.97873	0.01023	0.57469	0.01023	236.554	0.261	203.579	0.255
IB4W04J6Q	2010-06-01T22:44:58.5	Kerberos	−1.96867	0.00800	0.59739	0.00800	239.657	0.202	205.975	0.201
IB4W01I9Q + 3	2010-04-24T07:52:34.0	Styx	0.40822	0.01253	1.54237	0.01253	296.226	0.315	238.165	0.317
IB4W02FQQ + 3	2010-05-21T16:38:14.0	Styx	0.78648	0.01388	−1.75753	0.01388	241.683	0.325	301.881	0.373
IB4W03FBQ + 3	2010-05-24T22:55:14.0	Styx	−0.52693	0.01000	−1.32187	0.01000	229.357	0.253	268.886	0.251
IB4W05YOQ + 3	2010-06-11T07:53:33.0	Styx	−1.37252	0.01128	1.06553	0.01128	277.432	0.267	218.135	0.300
IB4W06YWQ + 3	2010-06-25T07:26:36.0	Styx	0.87972	0.00522	1.02195	0.00522	257.810	0.140	307.669	0.123
IB4W07IYQ + 3	2010-07-02T20:03:24.0	Styx	−0.18719	0.00950	−1.95286	0.00950	249.546	0.230	213.355	0.248
IB4W08GYQ + 3	2010-07-06T02:21:04.0	Styx	−1.19326	0.01260	−0.68773	0.01260	281.498	0.260	247.090	0.366
IB4W09W0Q + 3	2010-07-14T21:06:19.0	Styx	0.65524	0.00924	1.30415	0.00924	221.222	0.244	281.018	0.222
IB4W10GSQ + 3	2010-07-24T17:40:03.0	Styx	−0.58326	0.01019	−1.37974	0.01019	282.116	0.265	235.969	0.249
IB4W11K2Q + 3	2010-08-14T10:29:41.0	Styx	−0.88937	0.00529	−1.09922	0.00529	284.331	0.109	245.174	0.154

A sample of the new Hubble astrometry for Charon, Nix, Hydra, Kerberos, and Styx. Supplementary material lists all available measurements. The astrometry data are given in (Δα cos(δ), Δδ) and (x,y) format which corresponds to relative measurements of satellite's position with respect to Pluto's reference position. The image mid-time (at Earth) was originally calculated in seconds TDB, as derived from the SPICE toolkit. In this table, the time tag been converted to UTC time format. The formal uncertainities (σ) originate from the image reduction procedure and they are in general tighter from what was actually used in the orbital fit.

underlying gradient in background light, we added to the model a 2-D polynomial of up to second order, and simultaneously fitted the parameters describing this background. For each measurement, we also created a mask array to identify corrupted pixels such as cosmic ray hits on the detector and nearby background stars. We performed each fit iteratively, by adding to the mask at each step any pixel whose residual, relative to the root-mean-square (rms) of the previous fit, was larger by a factor of ~10. We found this procedure to be very successful at identifying and excluding corrupted pixels, so that only valid pixels usually contributed to the fit. The mask generally stopped changing after one or two iterations. Upon completion, the covariance matrix of the fit, combined with the rms residual, provided us with formal error ellipse in our (x, y) position measurements. These values are also listed in Table 6 and in Supplementary Tables 2–5.

We could assess the success of our astrometric fit based on the rms residual between original image pixels and the model, after masked pixels had been excluded. For images with the same exposure time and filter, these residuals were generally very similar. However, occasionally the fit would fail because of cosmic ray hits or background stars landing close to the satellite being measured. These measurements could be easily identified because the rms residuals would be at least 2–3 times larger than in adjacent images. These corrupted measurements were excluded from further analysis and do not appear in the tables.

Our measurements proceeded in phases, beginning with Pluto and working downward to the smaller, fainter bodies. We fitted a PSF model for Pluto to a 41 × 41 square of pixels surrounding its position. We then used this model to subtract Pluto from the image. Pluto is saturated in our longest exposures, but we applied

this technique regardless of saturation. The saturated pixels were treated as part of the mask of excluded pixels during the fitting procedure. This process was still successful at suppressing Pluto's glare even in saturated images. However, we have deemed our Pluto astrometry from saturated images to be less reliable, and have not included these measurements in our analysis.

Next, we performed the same analysis for Charon, using a 21×21 square of pixels. We then measured and subtracted Hydra and Nix using 11×11 squares, and finally Kerberos and Styx using 9×9 squares. The reason to shrink the box size for fainter bodies is that we wanted each position measurement to be dominated by the pixels in which the body was most detectable, and fainter bodies become undetectable within a smaller radius of their central pixel.

The Tiny Tim software provides a range of options including one called "jitter", which convolves the PSF with a 2-D Gaussian of specified standard deviation in mas. We experimented with this parameter to determine how best to handle the marginally resolved disks of Pluto ($\sim$2 pixels) and Charon ($\sim$1 pixel). To our surprise, we found that, nonzero values of jitter always produced more accurate models for the PSFs. For example, Hydra and Nix are unresolved, and yet jitter = 20 mas always produced a cleaner subtraction of their PSFs from the images than did jitter = 0. We interpret this as a modest shortcoming of the models for HST's optics employed by Tiny Tim. In the end, we used jitter = 40 mas for Pluto, 30 mas for Charon, and 20 for the smaller bodies. Note, for comparison, that the UVIS pixel scale is approximately 40 mas, whereas the HRC pixel scale is 25 mas.

Pluto, Charon, Nix and Hydra were always obvious objects in the images we analyzed. Kerberos and Styx, however, required considerably greater effort. In the longest exposures, Kerberos and Styx could often be seen in individual images, particularly after the brighter objects had been subtracted. In others, co-adding was necessary. Here we would take advantage of the fact that the moons move very little within a single $\sim$50-min observing period of HST. Even then, our procedure involved some iteration, where we would fit a rough, Keplerian orbit to the measurements in hand, and use that orbit to predict the locations where Kerberos and Styx were expected to fall in other images. This procedure enabled us to identify some very marginal detections of the tiniest moons. Table 1 in the Supplementary material identifies which of the measurements were obtained from co-added images via a suffix "+N" on the image ID. Here the ID identifies the first image of the set, and N indicates the number of subsequent images with identical exposure time and filter that were co-added to produce the final result. In the 2010 data set, some of the images were combined in spite of dither steps (i.e., pixel shifts) that had been performed in between the exposures. Images were aligned to the nearest whole pixel, so these measurements produced slightly blurred images of Kerberos and Styx. Nevertheless, we obtained numerous pre-discovery detections of both moons.

For the measurements to be useful for astrometry, we need to convert pixel (x, y) coordinates and their uncertainties to sky coordinates (α, δ). We perform this transformation using standard polynomial models for the distortion of each image, combined with pointing and rotational information embedded within the headers of all HST images. This information is suitable for obtaining relative position measurements at the sub-pixel scale we require, even though the absolute pointing remains uncertain at the level of arcseconds.

However, relative astrometry usually depends on the expectation that measurements have been obtained simultaneously, from the same image. This assumption is violated in our data set, because measurements of Kerberos and Styx, in particular, often require co-adding multiple images, whereas Nix and Hydra are visible in most individual frames. Furthermore, the best astrometry

of Charon and Pluto comes from short, unsaturated exposures, but these images are generally not suitable for precise astrometry of the smaller moons.

We have adopted a new procedure to "weave together" all of the astrometry from a single orbit of HST, enabling our measurements of all six objects to be inter-compared with full precision. We take advantage of HST's extremely precise pointing stability during a single Earth orbit, which typically comprises 45–50 min of observing time. HST's nominal precision during one orbit is 3 mas, and in practice we find it to be generally even finer. This precision applies even when HST is tracking a moving target (in this case, Pluto), and even when allowing for dither steps (which are small, commanded pointing changes in between the images of an orbit). Because of HST's precise tracking, we can always extrapolate the positions of Pluto and Charon from the images in which these bodies can be measured into images in which they cannot. In practice, we take all of our best astrometry of Pluto and Charon, sometimes supplemented with that of Nix and Hydra, to derive Pluto's "reference position" in each image (we use the latest available ephemeris from JPL, PLU042, for this purpose). Once this reference position has been defined, we tabulate all measurements as offsets in (α, δ) from this point. It remains possible that our reference position is off in absolute terms due to an ephemeris error, but any tracking errors among our astrometry measurements, even those obtained from different images or from different co-additions of the same images, will be limited to $\sim$3 mas.

In Table 1 of the supplement, sets of images with a common proposal ID, visit number and orbit number all fall within the same orbit. The adopted reference points are given as image coordinates (x, y) and as sky coordinates (α, δ). Here integer values of x and y refer to the center of a pixel, where the center of the image's lower left pixel is (0,0). As discussed below, we accommodate the possible absolute error in our reference position by solving for a bias in (α, δ), which we assume to be constant for all of the measurements obtained from the same orbit. These biases also compensate for another (few miliarcseconds) systematic effect: the difference between the astrometry being "relative to Pluto's reference position" as opposed to being "relative to Pluto's measured position". Note that the old astrometry in Tables 1–4 is assumed to be "relative to Pluto's measured position" and only the new astrometry is different. We argue that both astrometry methods are equivalent up to a positional bias that can easily be accounted for in the orbital fitting procedure.

Formally, the covariance matrix returned by the fitting procedure returns an error ellipse, defined by the uncertainty in the (x, y) coordinates and the correlation between them. This ellipse would then need to be transformed into a different uncertainty ellipse in (α, δ) coordinates. In practice, however, we found that our error ellipses were almost always very nearly circles, with the uncertainties in (x, y) nearly equal and showing very small correlations. As a result, we opted to simplify the analysis by treating our uncertainties in (α, δ) as equal, uncorrelated values. This was accomplished by defining uncertainty radius as equal to the root-mean-square of the (x, y) uncertainties, and then transforming this single value from pixel coordinate to sky coordinates. As a result, the sky uncertainties are always equal in each row of Table 6.

2.3. Data weights

The data weights reflect the quality of the measurements; numerically, they are calculated as the inverse of the measurement's standard error, σ. Initially, we used the reported observation uncertainties to calculate the data weights, but during the course of our analysis we had to revise some of these weights. Our guiding criterion was that the weighted rms of the residuals for same-observer data remains within 15% of one. A smaller

number would mean that the data are under-weighted while a larger number would mean that the data are too tightly weighted. We did not change the initial weights if the same-observer data set contained fewer than 6 points or if the data already had very tight weights (<5 mas). A few points had very large residuals > 3σ and were removed altogether.

3. Methods

3.1. Albedo model

Pluto's surface albedo distribution has a strong systematic effect on the measurements of satellites' positions relative to Pluto (Tholen and Buie, 1997; Buie et al., 2010). We used the Buie et al. (2010) F555W ACS/HRC bidirectional V-band reflectance map of the surface of Pluto to correct most of Pluto-centered astrometry from center-of-light to center-of-figure (presumed to be center-of-mass). The albedo map was oriented with the pole that differs from the usual IAU pole for Pluto (M. Buie, personal communication): $\alpha = 133.02$ deg, $\delta = -9.09$ deg. The location of the prime meridian is calculated from $\omega = \omega_0 + nt$, where ω_0 is the longitude of the prime meridian at the J2000.0 epoch, n is the mean longitude rate and t is the time in days since J2000.0. The values used for the prime meridian and the rate are $\omega_0 = 303.230$ deg and $n = 56.3623195$ deg day^{-1} respectively. Note that the albedo model is applied as a part of the orbital fitting procedure and that all astrometry in Table 6 and in Supplementary Tables 2–5 are reported in their original, uncorrected format.

We discussed in Section 2.2 the difference between the old measured-Pluto relative astrometry and the new reference-Pluto relative astrometry. We argue that the albedo correction for the new astrometry is necessary given that the extrapolation of the Pluto's reference points starts from the measured Pluto position. Hence, all subsequent reference-Pluto relative measurements are affected by the albedo and need to be corrected for it.

We did not apply the albedo map to the old photographic plates and speckle astrometry for Charon given that the uncertainties in these data are much larger (>100 mas) than any albedo effects. We instead used a set of observer-dependent position angle biases. Furthermore, the older HST data (Null et al., 1993; Null and Owen, 1996) have been already corrected with the earlier albedo model (Buie et al., 1992), so we kept these measurements in their published format.

3.2. Lightcurves model

We approximate shapes of lightcurves for the Pluto–Charon mutual events based on the Dunbar and Tedesco (1986) 3-circles overlap model. The three circles represent Pluto, Charon, and Pluto's or Charon's shadow. The mutual events occur in the plane perpendicular to the observer's line of sight to the eclipsed/occulted body. The model calculates area of the section (ΔA) of Pluto's or Charon's surface that is affected by the disk of occulting body and/or the shadow that belongs to that body. We used 1181.0 km for the radius of Pluto (Lellouch et al., 2009) and 605.0 km for the radius of Charon (Sicardy et al., 2006b; Gulbis et al., 2006; Person et al., 2006). In principle, we could have left the radii as floating parameters that get adjusted during the course of the fit, but we felt that the complexity of model is already substantial, and that it is unlikely that we would be able to constrain the radii beyond the results from stellar occultations.

The flux is calculated as:

$$F = 1 - \kappa(\Delta A / A_{\text{Total}}) \qquad (1)$$

where κ is the albedo of the occulted/eclipsed body and A_{Total} is the combined area of the two bodies.

Given that the albedo κ is already a floating parameter adjusted for each individual lightcurve, we did not find the justification to apply the previously discussed albedo map to the lightcurves.

The flux may be expressed in terms of magnitude:

$$F_{\text{mag}} = V_0 + 2.5\log_{10}(1 - F) \qquad (2)$$

with V_0 being the base magnitude. We also added a linear term $\eta\Delta t$ in order to account for slopes that appear in some of the lightcurves. Fig. 1 shows a sample of the fitted lightcurves, while the rest of the data are in the Supplementary material. The overall fits to the lightcurves are good, and although there could be some un-modeled albedo related signatures, their contributions to the fits are small.

3.3. Orbital fit

Our orbital model is a numerical integration of the equations of motion as described in Peters (1981). The integration uses Gauss-Jackson method with a variable order, variable step size. The integration step is controlled by the maximum acceptable error on the components of satellites' velocity vectors ($v_{\text{max}} = 10^{-10}$ km s^{-1}). The model includes external perturbations from the Sun, Jupiter, Saturn, Uranus, and Neptune, although these could be neglected for the satellites deep in the potential well of Pluto (Lee and Peale, 2006; Tholen et al., 2008). The model does not include Pluto's and Charon's gravitational harmonics J_2 and C_{22} because our first-order calculation that assumes a hydrostatic equilibrium and a simplified two-layer interior model (Rappaport et al., 2007) resulted in sub-km effects on the satellites' orbits (Supplementary material). JPL planetary ephemeris DE430 (Folkner et al., 2014) provides positions and GMs of the Sun and the planets (Table 7). The maximum order of integration is 15 and the average step size is 1200 s. We use bounded least-squares (BVLS) (Lawson and Hanson, 1995) algorithm in order to estimate the equation's dynamical parameters. BVLS solves linear least-squares problem with upper and lower bounds on the variables which prevented masses of Styx, Nix, Kerberos, and Hydra from becoming negative due to lack of strong mass signature in the data.

The parameters that are being estimated include the epoch position and velocity of each satellite in the International Celestial Reference Frame (ICRF) cartesian coordinates relative to the Pluto system barycenter, as well as the system's and satellites' GM values. In addition, we also solve for the observational model parameters. These include biases in right ascension and declination in Olkin et al. (2003) data to account for an error in the absolute position of the Pluto system barycenter, observer-dependent position angle biases for early photographic plates and speckle interferometry data, corrections to the position of the reference stars for Null et al. (1993) and Null and Owen (1996) HST data, an observational bias in Buie et al. (2012) HST data from April 2007 to June 2007 where Nix, Hydra, and Kerberos were measured with respect to Charon, positional biases in (α, δ) for all new astrometry grouped by the HST orbit, and all parameters in the lightcurve model. These additional parameters and their uncertainties help inflate the overall orbital uncertainties, and they ensure more conservative results (Jacobson, 2009).

4. Results

4.1. Postfit residual statistics

Tables 1–5 contain postfit residual statistics for observations grouped by the satellite and source. The rms of the residuals measures how well the orbital fit matched the data. There are four types of astrometric observations used in this study: ($\Delta\alpha\cos(\delta)$, $\Delta\delta$) – the tangential plane separation in right ascension and
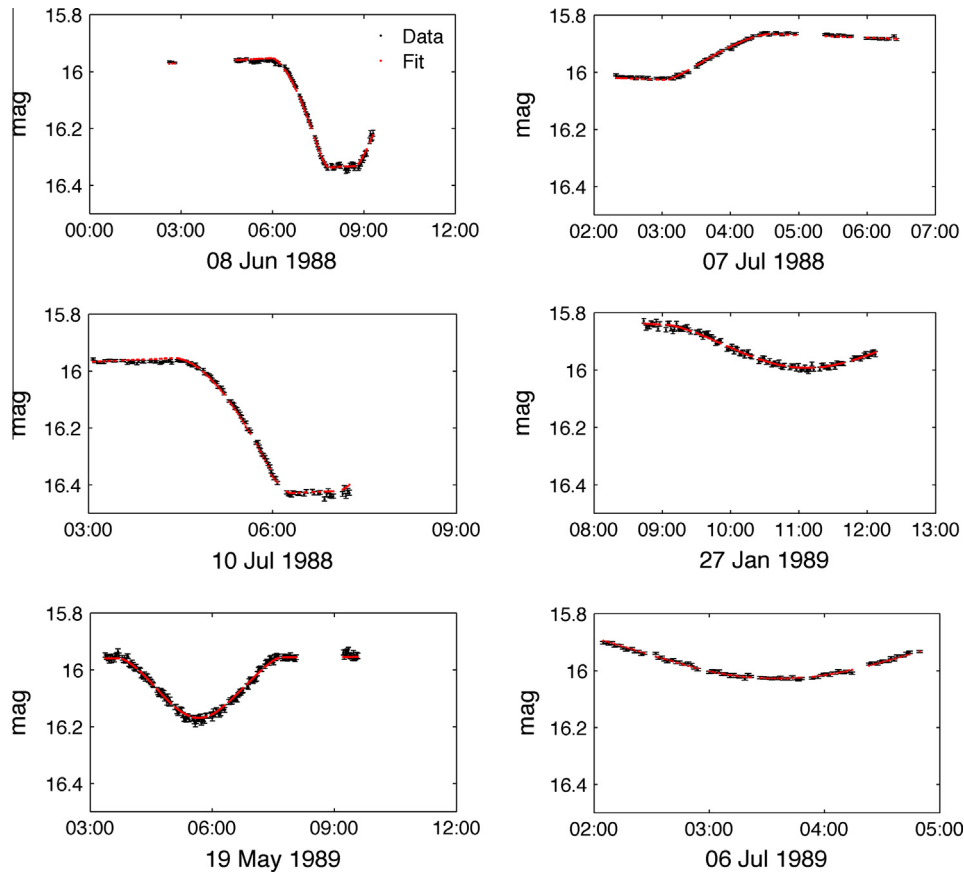
Fig. 1. Selected lightcurves of Pluto–Charon mutual events obtained by Mauna Kea Observatory (Tholen, 2008). The black dots mark the data with their errorbars, while the red dots mark the computed points. The rest of the lightcurves are in the Supplementary material.

Table 7
Dynamical constants.

Constant	Value	Reference
Jovian system GM (km³ s⁻²)	126712764.8000	Folkner et al. (2014)
Saturnian system GM (km³ s⁻²)	37940585.2000	Jacobson (2006)
Uranian system GM (km³ s⁻²)	5794568.6000	Jacobson et al. (1992)
Neptunian system GM (km³ s⁻²)	6836527.1000	Jacobson (2009)
Sun GM (km³ s⁻²)	132713233263.9000	Folkner et al. (2014)

List of the external perturbers that are included in the orbital integration.
The Sun's GM is augmented by the masses of the inner planets and the Moon.

declination between the satellite and a reference body; $(\Delta\theta, \Delta\rho)$ – satellite's position angle and separation from Pluto; (α, δ) – the absolute measurements of right ascension and declination of Charon, and CCD sample and line locations of Charon in the old HST data. For the case of position angle measurements, the final residuals and the rms of residuals were calculated as $\rho\Delta\theta$. As expected, rms for the pre-Hubble era data can be quite large ($\sim$100 mas), while the recent observations of Charon have rms below 10 mas. The rms statistics for Nix, Hydra, Kerberos, and Styx are on the order of 10 mas and better for the Hubble data and $\sim$100 mas for four Nix and Hydra points (Fuentes and Holman, 2006) that were obtained with Magelan I Baade telescope.

Another way to look at the goodness of an orbital fit is to directly display right ascension and declination residuals for each of the satellites (Figs. 2–6). Charon's observations span almost 50 years, and Fig. 2 shows how the quality of observations progressed from some very coarse astrometry in the pre-Hubble era to some very accurate points obtained with the Hubble and the

modern day telescopes. At this point, both Nix and Hydra have well constrained orbits and Figs. 3 and 4 show their residuals. The scatter of the residuals is within the assigned uncertainties, and there are no evident biases. Kerberos observations (residuals in Fig. 5) span almost 10 years thanks to some pre-discovery astrometry (see Supplementary material). Not surprisingly, Styx has the fewest astrometry points (residuals in Fig. 6) given its recent discovery in 2012 and some pre-discovery data from 2010 to 2011. The right ascension and declination residuals show scatter that is consistent with the data weights.

4.2. Epoch state vectors and mean orbital elements

We list state vectors in Table 8. The values have a precision of eleven and sixteen decimal places in order to allow for future orbit integrations. The epoch for all state vectors is January 1, 2013 barycentric dynamical time (TDB). TDB is the standard coordinate scale time in JPL's planetary and satellite ephemerides.

Orbital integration results are often easier to interpret in the form of mean orbital elements. We calculated mean orbital elements by fitting a precessing ellipse to 200 years of integrated orbits (Table 9). The reference plane is set to Charon's mean orbit and α = 133.03 deg, δ = −6.23 deg specify the direction of the orbit normal in ICRF. The epoch for the elements is January 1, 2000 TDB. Long orbital integration ensures that any periodic perturbations will average out. For the parameters listed in Table 9, a is the semi-major axis, e is the eccentricity, i is the inclination, λ is the epoch mean longitude, ϖ is the periapsis longitude, ω is the longitude of the ascending node, $d\lambda/dt$ is the mean longitude rate, $d\varpi/dt$ is the longitude of periapsis rate, and $d\omega/dt$ is the nodal rate. The
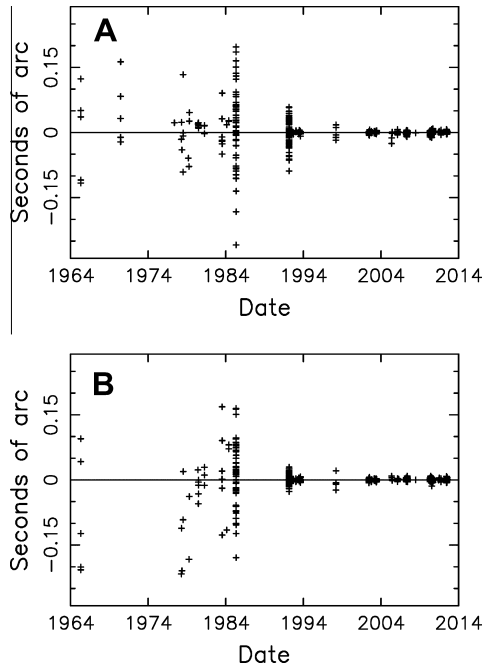
Fig. 2. (A) Charon's Right Ascension Residuals, $\Delta\alpha\cos(\delta)$. (B) Charon's Declination Residuals, $\Delta\delta$.
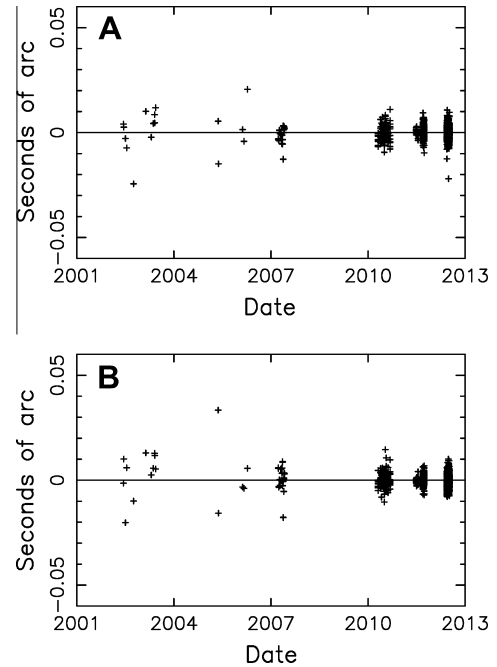

Fig. 4. (A) Hydra's Right Ascension Residuals, $\Delta\alpha\cos(\delta)$. (B) Hydra's Declination Residuals, $\Delta\delta$.
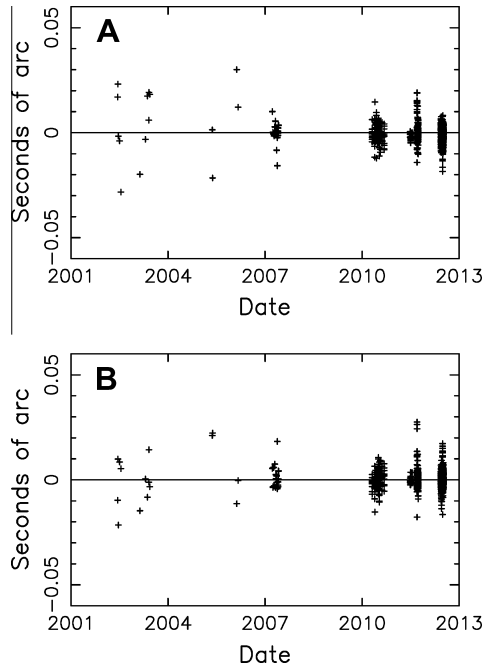

Fig. 3. (A) Nix's Right Ascension Residuals, $\Delta\alpha\cos(\delta)$. (B) Nix's Declination Residuals, $\Delta\delta$.
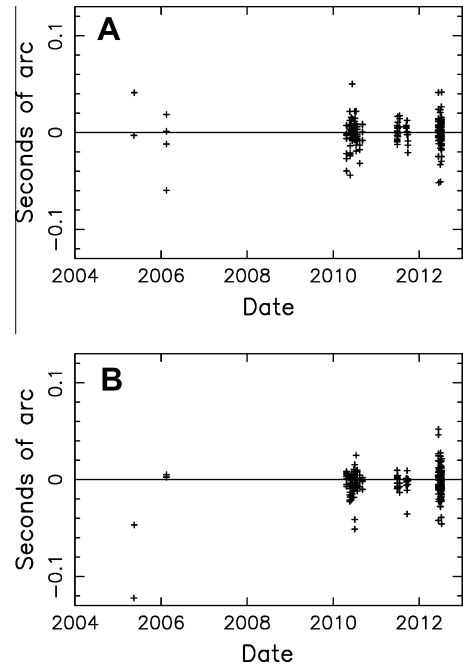

Fig. 5. (A) Kerberos's Right Ascension Residuals, $\Delta\alpha\cos(\delta)$. (B) Kerberos's Declination Residuals, $\Delta\delta$.

elements are planetocentric for Charon and barycentric for other satellites. We do not list any uncertainties associated with the mean elements because they are a true representation of the integrated orbits. The question of how well the integrated orbits represent the data has already been discussed in the previous section, and an estimate of their uncertainties will be discussed in an upcoming section.

Table 9 shows that the orbit of Charon is almost circular with an eccentricity of 5.1×10^{-5}. This is consistent with the Buie et al. (2012) upper limit on Charon's eccentricity of 7.5×10^{-5}.

Table 9 also lists mean orbital elements for Styx, Nix, Kerberos, and Hydra. Orbits of Nix and Kerberos are very close to a circle while Hydra's orbit appears to have a detectable eccentricity ($e = 0.00554$). This eccentricity is consistent with what was predicted ($e_{\text{Hydra}} = 0.0052$) by theoretical models of Lee and Peale (2006). The nodal and apsidal precession rates are not well constrained in the current fits due to the small sizes of orbital eccentricities and inclinations. Hydra and Kerberos seem to have significant enough inclinations and/or eccentricities that the rates are starting to have reasonable values. At their distances, Charon's
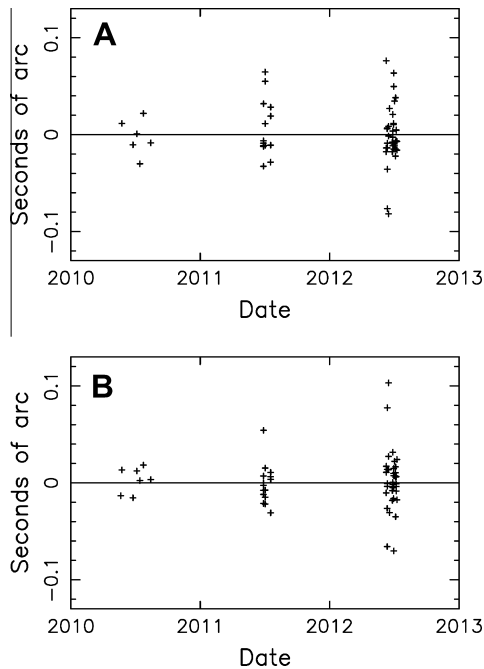
Fig. 6. (A) Styx's Right Ascension Residuals, $\Delta\alpha\cos(\delta)$. (B) Styx's Declination Residuals, $\Delta\delta$.

Table 8
State vectors for the satellites of Pluto.

Satellite	Position (km)	Velocity (km s^{-1})
Charon	1297.17438478526	0.1453959508510873
	3752.60226174718	0.1297771902069882
	17011.90583845352	−0.0397230039699411
Styx	−30572.84277725838	0.0232883188913688
	−26535.81343448966	0.0427977975396927
	12311.29089587663	0.1464990283534413
Nix	9024.34878023784	0.1004334400015913
	15210.73701650077	0.0865524814427462
	45591.75735722126	−0.0479498746416020
Kerberos	23564.20702505210	0.0792537025667567
	28380.03995076242	0.0630220099842493
	44578.02582182780	−0.0817084451068904
Hydra	−43331.32611324427	−0.0374001037580065
	−43628.45759453865	−0.0184905610710285
	−20506.54193573317	0.1157937282701088

Satellites' position (x,y,z) and velocity (v_x, v_y, v_z) are given in the International Celestial. Reference Frame (ICRF) cartesian coordinates relative to the Pluto system barycenter. The epoch for the state vectors is January 1, 2013 TDB.

Table 9
Mean equatorial orbital elements for the satellites of Pluto.

Element	Charon	Styx	Nix	Kerberos	Hydra
a (km)	19596	42413	48690	57750	64721
e	0.00005	0.00001	0.00000	0.00000	0.00554
ϖ (deg)	189.9	17.8	–	–	258.0
λ (deg)	276.0	180.5	85.0	261.9	228.4
i (deg)	0.0	0.0	0.0	0.4	0.3
Ω (deg)	–	–	–	313.3	122.7
$d\lambda/dt$ (deg day^{-1})	56.3625	17.8556	14.4841	11.1913	9.4236
$d\varpi/dt$ (deg year^{-1})	–	–	–	–	25.6970
$d\Omega/dt$ (deg year^{-1})	–	–	–	−39.7988	−25.7980
P (days)	6.3872	20.1617	24.8548	32.1679	38.2021

Mean orbital elements are derived based on 200 years of orbital integration. The epoch for the elements is JED 2451544.5. Charon's mean orbital elements are plutocentric while Styx's, Nix's, Kerberos', and Hydra's mean orbital elements are barycentric. Here, a is the semimajor axis, e is the eccentricity, i is the inclination, λ is the mean longitude, ϖ is the periapsis longitude, $d\lambda/dt$ is the mean longitude rate, $d\varpi/dt$ is the longitude of periapsis rate, and $d\omega/dt$ is the nodal rate. We also list the orbital period in days (P). The reference plane is set to Charon's mean orbit that has the orbit normal at α = 133.03 deg and δ = −6.23 deg in ICRF.
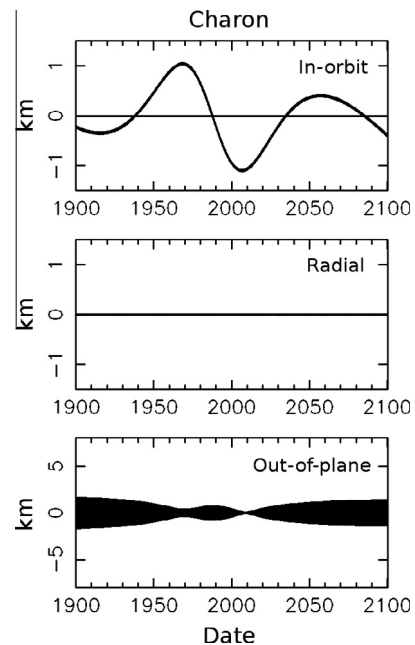

Fig. 7. Charon's in-orbit, radial, and out-of-plane differences (in km) between the elliptical and integrated orbits. The periodic signature is due to the Sun.

orbit around Pluto simulates a large J_2 in the gravitational field that results in precession of the periapsides and regression of the nodes. It is interesting to note that our value for Hydra's precession period ($\sim$5117 days) is not far from the period predicted by the Lee and Peale (2006) analytical theory ($\sim$5300 days).

Figs. 7 and 8 show differences between the integrated and elliptical orbits over 200 years. Charon's orbit (Fig. 7) remains very close to an ellipse for this period of time. We have traced the origin of the sinusoidal, $\sim$1 km in-orbit variations as well as the few km out-of-plane variations to the solar perturbations. On the other hand, Charon is the primary cause for the "bandwidths" of the in-orbit, radial, and out-of-plane differences for Styx, Nix, Kerberos, and Hydra in Fig. 8. Note how the out-of-plane differences decrease as the distance from Charon increases. In addition, all small satellites show the secondary long-term patterns that are superimposed on top of

the wide swath of orbital differences caused by Charon. We analyzed the origin of these differences with models where different combinations of satellites besides Charon would have mass(es). A comparison between the models revealed that the masses of Nix, Kerberos, and Hydra cause the secondary patterns. For example, the in-orbit difference for Styx shows a strong sinusoid modulation due to presence of Nix. Similarly, there is another sinusoid pattern superimposed on the in-orbit differences for Kerberos due to combined influences of Nix and Hydra. In return, Kerberos also perturbs Nix and Hydra. In summary, we are looking at a system of satellites that gravitationally interact in a complex way.

4.3. Satellite masses and densities

The system mass and the masses of satellites were treated as free parameters and were solved for simultaneously with other
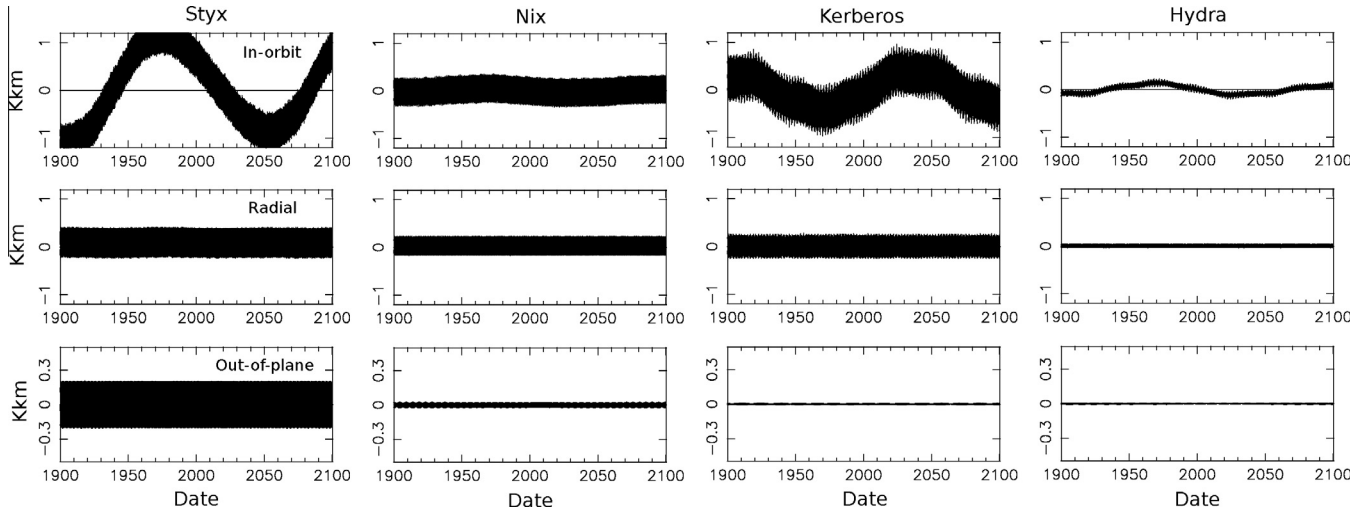
Fig. 8. Styx's, Nix's, Kerberos', and Hydra's in-orbit, radial, and out-of-plane differences (in Kilo-km) between the elliptical and integrated orbits.

dynamical quantities. The mass of Pluto is calculated as a dependent quantity after the fit. The current orbital fit gives some very tight constraints on Charon's and system's GMs: GM_{system} = 975.5 ± 0.2 km^3 s^{-2} and GM_{Charon} = 105.9 ± 0.3 km^3 s^{-2}. 1σ errors are obtained based on the formal covariance from the fit and they reflect random measurement errors as opposed to systematic errors. However, each data set comes with its inherent systematic errors, and if these data are abundant and tightly weighted, they may even dominate the fit. We have tried to offset this issue by comparing the fits from the subsets of data. Our conclusion was that the system and Charon mass uncertainties need to be significantly inflated in order to account for any systematic effects: GM_{system} = 975.5 ± 1.5 km^3 s^{-2} and GM_{Charon} = 105.9 ± 1.0 km^3 s^{-2}. Similar argument is also valid for the small satellites, although their formal 1σ errors appear to be large enough to encompass any systematic effects for now. Mass estimates and their associated uncertainties are summarized in Table 10.

Hydra and Nix have comparable masses in the current fit, GM_{Hydra} = 0.0032 ± 0.0028 km^3 s^{-2} and $GMNix$ = 0.0030 ± 0.0027 km^3 s^{-2}, although the uncertainties remain large. The mass values are consistent with the upper bounds that Youdin et al. (2012) predicted based on the orbital stability of Kerberos (0.0033 km^3 s^{-2} for Nix and 0.0060 km^3 s^{-2} for Hydra). Given the uncertainties in the results of our orbital fit, it would not be surprising if the mass of Hydra increases while the mass of Nix decreases with the addition of future data. The new HST astrometry reported in this paper also produced an order-of-magnitude estimate for the mass of Kerberos ($GM_{Kerberos}$ = 0.0011 ± 0.0006 km^3 s^{-2}). Table 10 shows that the mass of Styx remains at zero, but with an upper bound of 0.0010 km^3 s^{-2}.

Pluto's and Charon's densities have been estimated in multiple analyses (Null et al., 1993; Young et al., 1994; Null and Owen, 1996; Tholen et al., 2008). The dominant source of the uncertainty for Pluto's density has always been its radius, while for Charon, the dominant source of density uncertainty has been its mass. In this analysis, Charon's density is still dominated by the mass uncertainty, if only slightly. For Pluto, we obtain ρ_{Pluto} = 1.89 ± 0.06 g cm^{-3} and for Charon, ρ_{Charon} = 1.72 ± 0.02 g cm^{-3}. It is difficult to discuss the densities for other satellites given that there are still large uncertainties associated with their masses and their sizes are virtually unknown. However, if we take the masses from Table 10 at their "face value" and assume a range of diameters based on the high (35%) and low (4%) geometric albedo limits, some conclusions may be drawn about the potential range of densities. The upper

Table 10
Masses and densities in the Pluto system.

Object	GM (km^3 s^{-2})	R (km)	ρ (g cm^{-3})
System	975.5 ± 1.5	–	–
Pluto	869.6 ± 1.8	1169–1193[a]	1.89 ± 0.06
Charon	105.88 ± 1.0	603.6 ± 1.4[b]	1.72 ± 0.02
Styx	$0.0000^{+0.0010}_{-0.0000}$	4–14	–
Nix	0.0030 ± 0.0027	23–70	<1.68
Kerberos	0.0011 ± 0.0006	7–22	–
Hydra	0.0032 ± 0.0028	29–86	<0.88

The system mass and masses of the individual satellites are estimated from the orbital integration. Pluto's mass is calculated from the system and satellites masses. The errors represent formal 1σ uncertainty for the masses of Styx, Nix, Kerberos, and Hydra. The errors for system's and Charon's mass have been inflated in order to account for the systematic effects (see Section 3.2). Sizes of the smaller satellites were estimated based on Russell (1916) equation as described in Steffl et al. (2006). The high and low visual geometric albedos were 35% and 4% respectively. We used the following visual magnitudes: V_{Styx} = 27.00 (Showalter et al., 2012), V_{Nix} = 23.38 (Weaver et al., 2006), $V_{Kerberos}$ = 25.95 (an average of what was reported in Showalter et al. (2011)), and V_{Hydra} = 22.93 (Weaver et al., 2006). The densities are calculated based on the nominal mass and the average radius for Pluto and Charon. The errors on the densities are calculated from the errors on masses and radii. We calculate the upper bounds on densities of Nix and Hydra based on their maximum masses and minimum radii (the lower limits have densities close to zero, which are unrealistic results). The densities of Styx and Kerberos remain unconstrained.
^a [a] Lellouch et al. (2009).
^b [b] Sicardy et al. (2006b).

bound on the density of Hydra, 0.88 g cm^{-3}, implies that the satellite could be significantly less dense than Charon. We note that the "high-end" density is calculated with GM_{Hydra} = 0.0060 km^3 s^{-2} which is already at the upper dynamical limit as constrained by Youdin et al (2012). The current upper bound for the density of Nix is 1.68 g cm^{-3}, although we expect that the true value is likely lower and closer to the density of Hydra (<1 g cm^{-3}). The upper bound is calculated with GM_{Nix} = 0.0057 km^3 s^{-2} which is much higher than what the dynamical limit due to the stability of Kerberos implies (GM_{Nix} < 0.0030 km^3 s^{-2}, Youdin et al. (2012)). The densities of Kerberos and Styx remain largely unconstrained at this point, given that the most extreme cases of their mass/radius combinations do not produce physically meaningful quantities.

4.4. Orbital uncertainties

Jacobson et al. (2012) showed that random and systematic errors in observations dominate the orbital uncertainties and that

mapping of the covariance matrix obtained from the least-squares fit represents a method for placing a reasonable bound on the position of a satellite at some later time. Orbital uncertainty estimates are particularly important when planning the upcoming encounter of the New Horizons spacecraft with the Pluto system in July of 2015. In order to quantify the uncertainties in our orbital fit, we project the mapped covariance of each satellite state along three directions: in-orbit, radial, and the out-of-plane (Table 11). In-orbit (or along the track) uncertainties reflect the uncertainties in longitude and eccentricity, radial uncertainties are correlated with the uncertainties in semimajor axis and eccentricities, and out-of-plane errors reflect inclination and node errors. At the time of the encounter, Charon's location can be determined within ten kilometers, Nix and Hydra are uncertain to within few tens of km, while Kerberos and Styx have more than 100 km uncertainties in their positions. The predicted orbital position error is largest along the satellite's orbit due to the uncertainty in mean motion. The uncertainties along the directions perpendicular to the down-track are much smaller. Orbital uncertainties for Nix and Hydra listed in Table 11 are compatible with the predictions from Buie et al. (2013). They used two-body orbital fits to the HST astrometry from 2002 to 2010, which is obviously more limited dataset than what was used here, so it is not surprising that Table 11 lists tighter orbital constrains.

5. Discussion

Charon's mass is well constrained in the current fit even with our decision to inflate the formal 1σ error in order to include potential systematic errors (from $GM_{Charon} = 105.9 \pm 0.3$ km^3 s^{-2} to $GM_{Charon} = 105.9 \pm 1.0$ km^3 s^{-2}). The mass sensitivity largely comes from the substantial amount of astrometry of the small satellites. For example, if we only fit Charon's data, the mass of Charon remains relatively poorly constrained ($GM_{Charon} = 105 \pm 3.9$ km^3 s^{-2}, formal 1σ from the covariance). This is not surprising considering that the mass arises from a handful of absolute astrometry points from Null et al. (1993), Null and Owen (1996), and Olkin et al. (2003). Charon's mass becomes better and better constrained with addition of each year of astrometry from the small satellites. We were not able to identify any resonant arguments between Charon, Nix, and Hydra based on the orbital elements and rates in Table 10. We later extended the search for resonance with Kerberos and Styx, but none were found. Furthermore, we tried to search for resonances with the theoretical values for the apsidal and nodal rates given that the values in Table 10 are not well constrained due to small eccentricities and inclinations, but no candidates emerged.

The evidence for masses of the small satellites is still subtle in the current data. The rms of the residuals remains almost unchanged between the orbital fit where only Charon has a mass and the one listed in Table 10. When we compared the two solutions for the in-orbit, radial, and out-of-plane directions, orbits of Styx, Nix, Kerberos, and Hydra differed by several tens to a hundred kilometers. The largest difference was always in the in-orbit

Table 11
Orbital uncertainties for the satellites of Pluto.

Object	In-orbit (km)	Radial (km)	Out-of-plane (km)
Charon	5	6	2
Styx	514	50	187
Nix	23	11	16
Kerberos	135	21	57
Hydra	29	10	17

In-orbit, radial and out-of-plane orbital uncertainties at the time of New Horizons encounter (July 14, 2015). The uncertainties are estimated based on mapping of the covariance.

direction, signaling the change in the mean motion. However, even 100 km difference means little for the current data accuracy. At Pluto's distance, 1 arcsec $\sim$ 21,800 km, which means that the measurement error needs to be better than 5 mas in order to detect 100 km difference in the orbit. Styx and Kerberos are the most sensitive to any mass changes due to their proximity to Nix and Hydra, but the accuracy of their astrometry remains relatively low (>10 mas) in the current dataset.

Given the current status of orbital fits, it is natural to ask if any of the smaller satellites were serendipitously included in any of the 64 lightcurves obtained from 1985 to 1990. We found no evidence for the presence of Nix and Hydra, but it is possible that Kerberos and Styx could have been in the field of view on March 22, 1987 (Styx, superior event), July 25, 1987 (Kerberos, inferior event), and April 18, 1988 (Styx, inferior event). The latest orbital solutions for Kerberos and Styx still contain large uncertainties (especially for Styx), so we have considered a possibility of a mutual event whenever the satellite approached within 500 km on the plane-of-sky from Pluto. With the geometric conditions for mutual events satisfied, the question remains if a small, faint satellite could produce a detectable signature in Pluto–Charon lightcurves. Tholen et al. (2008) discussed if the very subtle post-eclipse brightening on April 18, 1988 could be due to a presence of a second satellite in the mutual event, and we have indeed found that Styx could be the culprit, but the overall evidence for a satellite in addition to Charon is weak.

We have shown that the current orbital solution provides good constraints (Table 11) on all but orbit of Styx. This will be particularly valuable for scheduling various instruments during the New Horizons flyby in July of 2015. It is important to note that the uncertainties in Table 11 are relative to Pluto and that the absolute position uncertainty must include Pluto's position uncertainty that is currently $\sim$2200 km (Folkner et al., 2014). With the addition of the new astrometry data (Earth-based, HST, or directly from the New Horizons camera), it is likely that the orbital uncertainties for Pluto and its satellites will improve by the time of the spacecraft flyby.

6. Conclusions

Satellites of the Pluto system have been studied for a while now, and their orbits have been fit with some very sophisticated dynamical models (Tholen et al., 2008; Beauvalet et al., 2013). Our analysis represents the latest orbit fitting effort where we used the most complete data set to date and most complete dynamical and observational models. This is the first time that the lightcurves from Pluto–Charon mutual events have been combined with other forms of astrometry. This is also the first time that the Pluto albedo effects were taken into account for the astrometry that spans several decades. We have also contributed a substantial set of the new HST astrometry for all satellites. The length of the data arc has significantly improved the orbital and mass uncertainties, and this is the first analysis where Kerberos and Styx were fitted with integrated orbits. Otherwise, most of the results of our analysis are consistent with what was already known about the satellites in the Pluto system. In the end, we would like to encourage astrometric observations of the Pluto's system both before and after the New Horizons flyby. The long data arc will assure for better orbital and mass constraints and we will be able to better understand the (near) resonant conditions in the system.

Pluto's satellites ephemerides (solution PLU043) are available from JPL's NAIF (http://naif.jpl.nasa.gov/naif/index.html) and Horizons (http://ssd.jpl.nasa.gov/?horizons).

Appendix A. Supplementary material

Supplementary data associated with this article can be found, in the online version, at http://dx.doi.org/10.1016/j.icarus.2014.03.015.

References

Baier, G., Weigelt, G., 1987. Speckle interferometric observations of Pluto and its moon Charon on seven different nights. Astron. Astrophys. 174, 295–298.

Baier, G., Hetterich, N., Weigelt, G., 1982. Digital speckle interferometry of Juno, Amphitrite and Pluto's moon Charon. ESO Mess. 23, 23–26.

Beauvalet, L., Robert, V., Lainely, V., Arlot, J.-E., Colas, E., 2013. ODIN: A new model and ephemeris for the Pluto system. Astron. Astrophys. 553, A14–A35.

Beletic, J.W., Goody, R.M., Tholen, D.J., 1989. Orbital elements of Charon from speckle interferometry. Icarus 79, 38–46.

Bonneau, D., Foy, R., 1980. Speckle interferometry with the 3.60 M CFH telescope. I – Resolution of the Pluto–Charon system. Astron. Astrophys. 92, L1–L4.

Buie, M.W., Tholen, D.J., Horne, K., 1992. Albedo maps of Pluto and Charon-Initial mutual event results. Icarus 97, 211–227.

Buie, M.W., Grundy, W.M., Young, E.F., Young, L.A., Stern, S.A., 2006. Orbits of Pluto's satellite. Astron. J. 132, 290–298.

Buie, M.W., Grundy, W.M., Young, E.F., Young, L.A., Stern, S.A., 2010. Pluto and Charon with the Hubble Space Telescope. II. Resolving changes on Pluto's Surface and a Map for Charon. Astron. J. 139, 1128–1143.

Buie, M.W., Tholen, D.J., Grundy, W.M., 2012. The orbit of Charon is circular. Astron. J. 144, 15 (19pp.).

Buie, M.W., Grundy, W.M., Tholen, D.J., 2013. Astrometry and orbits of Nix, Kerberos, and Hydra. Astron. J. 146, 152–164.

Buratti, B.J., Dunbar, R.S., Tedesco, E.F., Gibson, J., Marcialis, R.L., Wong, F., Bennett, S., Dobrovolskis, A., 1995. Modeling Pluto–Charon mutual events. II. CCD observations with the 60 in. telescope at Palomar Mountain. Astron. J. 110, 1405–1419.

Christy, J.W., Harrington, R.S., 1978. The satellite of Pluto. Astron. J. 83, 1005, 1007, 1008.

Dunbar, R.S., Tedesco, E.F., 1986. Modeling Pluto–Charon mutual eclipse events. I – First-order models. Astron. J. 92, 1201–1209.

Folkner, W.M., Williams, J.G., Boggs, D.H., Park, R.S., Kuchynka, P., 2014. The Planetary and Lunar Ephemerides DE 430 and DE 431. In: The Interplanetary Network Progress Report, vol. 42–196. Jet Propulsion Laboratory, Pasadena, CA. <http://ipnpr.jpl.nasa.gov/progress_report/42-196/196C.pdf>.

Foust, J.A., Elliot, J.L., Olkin, C.B., McDonald, S.W., 1997. Determination of the Charon/Pluto mass ratio from center-of-light astrometry. Icarus 126, 362–372.

Fuentes, C.I., Holman, M.J., 2006. Pluto Ii (Nix) and Pluto Iii (Hydra). CBET 602,1.

Gulbis et al., 2006. Charon's radius and atmospheric constraints from the 2005 July 11 stellar occultation. Nature 439, 48–51.

Harrington, R.S., Christy, J.W., 1980. The satellite of Pluto. II. Astron. J. 85, 168–170.

Hege, E.K., Drummond, J.D., 1984. Pluto. IAUC 3986, 1.

Hege, E.K., Hubbard, E.N., Drummond, J.D., Strittmatter, P.A., Worden, S.P., Lauer, T., 1982. Speckle interferometric observations of Pluto and Charon. Icarus 50, 72–81.

Hetterich, N., Weigelt, G., 1983. Speckle interferometry observations of Pluto's moon Charon. Astron. Astrophys. 125, 246–248.

Howell, S.B., Horch, E.P., Everett, M.E., Ciardi, D.R., 2012. Speckle camera imaging of the planet Pluto. Publ. Astron. Soc. Pac. 124, 1124–1131.

Jacobson, R.A. et al., 2006. The gravity field of the saturnian system from satellite observations and spacecraft tracking data. Astron. J. 132, 2520–2526.

Jacobson, R.A., 2009. The orbits of the Neptunian satellites and the orientation of the pole of Neptune. Astron. J. 137, 4322–4329.

Jacobson, R.A., Campbell, J.K., Taylor, A.H., Synnott, S.P., 1992. The masses of Uranus and its satellites from Voyager tracking data and Earth-based uranian satellite data. Astron. J. 103, 2068–2078.

Jacobson, R.A., Brozovic, M., Gladman, B., Alexandersen, M., Nicholson, P.D., Veillet, C., 2012. Irregular satellites of the outer planets: Orbital uncertainties and astrometric recoveries in 2009–2011. Astron. J. 144, 132–140.

Kenyon, S.J., Bromley, B.C., 2014. The formation of Pluto's low-mass satellites. Astron. J. 147, 8–25.

Krist, J.E., Hook, R.N., Stoehr, F., 2011. 20 years of Hubble Space Telescope optical modeling using Tiny Tim. In: Kahan, Mark A. (Ed.), Optical Modeling and Performance Predictions V. Proceedings of the SPIE, vol. 8127, 16pp. (article id. 81270J).

Lawson, C.L., Hanson, R.J., 1995. Solving Least Squares Problems (Revised edition). Society for Industrial and Applied Mathematics.

Lee, M.H., Peale, S.J., 2006. On the orbits and masses of the satellites of the Pluto Charon system. Icarus 184, 573–583.

Lellouch, E., Sicardy, B., de Bergh, C., 2009. Pluto's lower atmosphere structure and methane abundance from high-resolution spectroscopy and stellar occultations. Astron. Astrophys. 459, L17–L21.

Mutchler, M.J. et al., 2006. S/2005 P 1 and S/2005 P 2, IAUC 8676, 1.

Null, G.W., Owen Jr., W.M., 1996. Charon/Pluto mass ratio obtained with HST CCD observations in 1991 and 1993. Astron. J. 111, 1368–1381.

Null, G.W., Owen Jr., W.M., Synnott, S.P., 1993. Masses and densities of Pluto and Charon. Astron. J. 105, 2319–2335.

Olkin, C.B., Wasserman, L.H., Franz, O.G., 2003. The mass ratio of Charon to Pluto from Hubble Space Telescope astrometry with the fine guidance sensors. Icarus 164, 254–259.

Person, M.J. et al., 2006. Charon's radius and density from the combined data sets of the 2005 July 11 occultation. Astron. J. 132, 1575–1580.

Peters, C.F., 1981. Numerical integration of the satellites of the outer planets. Astron. Astrophys. 104, 37–41.

Pires dos Santos, P.M., Guliatti Winter, S.M., Sfair, R., 2011. Gravitational effects of Nix and Hydra in the external region of the Pluto–Charon system. Mon. Not. R. Astron. Soc. 410, 273–279.

Rappaport, N.J. et al., 2007. Mass and interior of Enceladus from Cassini data analysis. Icarus 190, 175–178.

Showalter, M.R., et al., 2012. New Satellite of (134340) Pluto: S/2012 (134340) 1, IAU Circ. 9253, 1.

Showalter, M.R., Hamilton, D.P., Stern, S.A., Weaver, H.A., Steffl, A.J., Young, L.A., 2011. New Satellite of (134340) Pluto: S/2011 (134340) 1. CBAT 2769.

Sicardy, B. et al., 2006b. Charon's size and an upper limit on its atmosphere from a stellar occultation. Nature 439, 52–54.

Sicardy, B. et al., 2006a. Pluto Iii (Hydra). CBET 610, 1.

Sicardy, B. et al., 2011. Constraints on Charon's orbital elements from the double stellar occultation of 2008 June 22. Astron. J. 141, 67–82.

Steffl, A.J. et al., 2006. New constraints on additional Satellites of the Pluto system. Astron. J. 132, 614–619.

Stern, S.A., Parker, J.W., Duncan, M.J., Snowdall Jr., J.C., Levison, H.F., 1994. Dynamical and observational constraints on satellites in the inner Pluto-Charon system. Icarus 108, 234–242.

Stern, S.A. et al., 2006. S/2005 P 1 and S/2005 P 2. IAUC 8686, 1.

Süli, A., Zsigmond, Zs., 2009. Detailed survey of the phase space around Nix and Hydra. Mon. Not. R. Astron. Soc. 398, 1–10.

Tholen, D.J. (Ed.), 2008. Pluto-Charon Mutual Events V3.0. EAR-A-3-RDR-PCME-V3.0. NASA Planetary Data System. <http://pds.nasa.gov/ds-view/pds/viewDataset.jsp?dsid=EAR-A-3-RDR-PCME-V3.0>.

Tholen, D.J., Buie, M.W., 1997. The orbit of Charon. Icarus 125, 245–260.

Tholen, D.J., Buie, M.W., Binzel, R.P., Frueh, M.L., 1987. Improved orbital and physical parameters for the Pluto–Charon system. Science 237, 512–514.

Tholen, D.J., Buie, M.W., Grundy, W.M., Elliot, G.T., 2008. Masses of Nix and Hydra. Astron. J. 135, 777–784.

Weaver, H.A. et al., 2006. Discovery of two new satellites of Pluto. Nature 439, 943–945.

Youdin, A.J., Kratter, K.M., Kenyon, S.J., 2012. Cicumbinary Chaos: Using Pluto's newest moon to constrain the masses of Nix and Hydra. Astrophys. J. 755, 17–28.

Young, E.F., 1992. An Albedo and Frost Model of Pluto. 1992 Ph.D. Thesis, Massachusetts Institute Technology.

Young, E.F., Binzel, R.P., 1993. Comparative mapping of Pluto's sub-Charon hemisphere: Three least-squares models based on mutual event lightcurves. Icarus 102, 134–149.

Young, L.A., Olkin, C.B., Elliot, J.L., Tholen, D.J., Buie, M.W., 1994. The Charon–Pluto mass ratio from MKO astrometry. Icarus 108, 186–199.